Phosphatidylinositol phosphate kinase type Iγ regulates dynamics of large dense-core vesicle fusion

Liang-Wei Gong*†, Gilbert Di Paolo*†, Ester Diaz‡, Gianluca Cestra*†, Maria-Elena Diaz‡, Manfred Lindau§, Pietro De Camilli*†¶, and Derek Toomre*‖

*Department of Cell Biology and †Howard Hughes Medical Institute, Yale University School of Medicine, New Haven, CT 06510; ‡Computer Science Department, University of Valencia, 50 Dr. Moliner, 46100 Burjassot, Spain; and §School of Applied and Engineering Physics, Cornell University, Ithaca, NY 14850

Contributed by Pietro De Camilli, February 18, 2005

Phosphatidylinositol-4,5-bisphosphate was proposed to be an important regulator of large dense-core vesicle exocytosis from neuroendocrine tissues. Here, we have examined the kinetics of secretion in chromaffin cells from mice lacking phosphatidylinositol phosphate kinase type Iγ, the major neuronal phosphatidylinositol-4-phosphate 5-kinase. Absence of this enzyme caused a reduction of the readily releasable vesicle pool and its refilling rate, with a small increase in morphologically docked vesicles, indicating a defect in vesicle priming. Furthermore, amperometry revealed a delay in fusion pore expansion. These results provide direct genetic evidence for a key role of phosphatidylinositol-4,5-bisphosphate synthesis in the regulation of large dense-core vesicle fusion dynamics.

exocytosis | fusion pore | granule | phosphatidylinositol-4,5-bisphosphate | secretion

Strong evidence has implicated phosphoinositides (PIs) in the regulation of membrane traffic, including exocytosis (1–4). A first clue suggesting a direct role of phosphatidylinositol-4,5-bisphosphate [$PI(4,5)P_2$] in secretion came from its requirement for Ca^{2+}-dependent exocytosis in broken chromaffin cells, independent from its phospholipase C (PLC)-mediated cleavage (5). Subsequently, a PI(4)P 5-kinase activity was implicated as a critical factor in the Ca^{2+}-activated secretion of large dense-core vesicles (LDCVs) from permeabilized PC12 cells, a chromaffin cell line (6). In addition, the molecular characterization of the exocytic machinery revealed that several proteins that directly or indirectly participate in the priming and fusion of neurosecretory vesicles contain $PI(4,5)P_2$-binding domains (1, 4, 7). For example, synaptotagmin, a putative Ca^{2+} sensor in the exocytosis of synaptic vesicles and LDCVs, binds $PI(4,5)P_2$ by means of C2 domains, and *in vitro* assays showed that this interaction is important in membrane fusion (8–10). Ca^{2+}-dependent activator for secretion (CAPS), which is required for Ca^{2+}-evoked LDCV secretion (11), binds $PI(4,5)P_2$ by means of a PH domain (12). Moreover, manipulations that artificially mask available $PI(4,5)P_2$, such as overexpression of a $PI(4,5)P_2$-binding module, the PH domain of PLCδ1, inhibits LDCV exocytosis (13, 14). Disruption of the function of Arf6, a positive regulator of $PI(4,5)P_2$ synthesis by means of its action on type I phosphoinositide-4-phosphate (PIP) kinases (15, 16), impairs neuroendocrine secretion (14, 17); conversely, stimulation of Arf6 enhances secretion (18). Diacylglycerol, a metabolic product of $PI(4,5)P_2$, is also implicated in synaptic vesicle and LDCV fusion with the plasma membrane (PM). Diacylglycerol, whose levels can be regulated not only by PLC-mediated cleavage of $PI(4,5)P_2$ but also by alternative metabolic pathways, binds to Munc13, and this interaction plays an essential role in the priming reaction of exocytosis (19–22).

$PI(4,5)P_2$ can be generated by type I and type II PIP kinases, which function as PI(4)P 5-kinases and PI(5)P 4-kinases, respectively (23). Type I PIP kinases are thought to account for the bulk of $PI(4,5)P_2$ synthesis, and there is evidence for a differential role of each type I PIP kinase isoform in the generation of functionally different $PI(4,5)P_2$ pools (24, 25). Recently, studies of knockout (KO; $-/-$) mice deficient in the expression of PIP kinase type Iγ (PIPKIγ), the main neuronal type I PIP kinase isoform, have demonstrated a decrease in $PI(4,5)P_2$ levels and $PI(4,5)P_2$ synthesis in neurons, which correlate with defects in both exo- and endocytosis of synaptic vesicles, and, therefore, in synaptic transmission both at excitatory and inhibitory synapses (26). The defects in synaptic vesicle exocytosis observed in these mice, which die shortly after birth, are suggestive of a decreased readily releasable pool (RRP) of vesicles (26). However, genetic information that proves the importance of $PI(4,5)P_2$ synthesis in the exocytosis of LDCVs in neuroendocrine cells is lacking. Furthermore, the key enzyme(s) involved in the generation of a pool of $PI(4,5)P_2$ potentially implicated in their exocytosis have not been identified.

In the present study, we have addressed the role of $PI(4,5)P_2$ synthesis in LDCV secretion from chromaffin cells by using adrenal glands of mice deficient in the expression of PIPKIγ. Our results reveal a role of $PI(4,5)P_2$ synthesis in vesicle priming and in the regulation of fusion dynamics.

Materials and Methods

Preparation of Embryonic Mouse Chromaffin Cells. The following solutions were prepared and sterile filtered (0.22 μm). Papain solution: 250 ml of DMEM (GIBCO) was supplemented with 50 mg of L-cysteine/1 mM $CaCl_2$/0.5 mM EDTA/20–25 units/ml papain (Sigma), and equilibrated with 5% CO_2. Inactivating solution: 225 ml of DMEM was supplemented with 25 ml of heat-inactivated FCS/625 mg of albumin/625 mg of trypsin inhibitor (Sigma, T-9253). Enriched DMEM: 500 ml of DMEM was supplemented with 5 ml of penicillin/streptomycin (Invitrogen)/5 ml of insulin-transferrin-selenium-X (Invitrogen). Adrenal glands were dissected from newborn wild-type (WT, $+/+$) or KO mice, placed in filtered Locke's solution (154 mM NaCl/5.6 mM KCl/3.6 mM $NaHCO_3$/10 mM glucose, pH 7.2). Contaminating tissue was removed by dissection. The glands were incubated in 1 ml of papain solution at 37°C for 40 min and inactivated by addition of 0.75 ml of the inactivating solution for another 10 min. The medium was carefully replaced with 0.2 ml of enriched DMEM and the glands were triturated gently through a 200-μl pipette tip. Seventy microliters of the cell

Freely available online through the PNAS open access option.

Abbreviations: PI, phosphoinositide; PIP kinase, phosphatidylinositol phosphate kinase; PIPKIγ, PIP kinase type Iγ; KO, knockout; LDCV, large dense-core vesicle; $PI(4,5)P_2$, phosphatidylinositol-4,5-bisphosphate; PLC, phospholipase C; RRP, readily releasable pool; PM, plasma membrane.

¶To whom correspondence may be addressed at: Department of Cell Biology, Howard Hughes Medical Institute, Yale University School of Medicine, 295 Congress Avenue, New Haven, CT 06510. E-mail: pietro.decamilli@yale.edu.

‖To whom correspondence may be addressed at: Department of Cell Biology, Yale University School of Medicine, SHM-C227/229, 333 Cedar Street, New Haven, CT 06520. E-mail: derek.toomre@yale.edu

aliquots was plated on 12-mm polylysine-coated coverslips, and cells were allowed to attach before supplementing with 2 ml of enriched medium. The cells were incubated at 37°C in 5% CO_2 and used within 4 days.

Biochemistry. Adrenal tissue was removed from newborn animals and immediately homogenized and solubilized in SDS/PAGE sample buffer. For PC12 cell cytosol extract, cells were homogenized in lysis buffer [25 mM Hepes (pH 7.4)/150 mM KCl/2 mM EGTA supplemented with a mixture of protease inhibitors] by using a Dounce homogenizer and centrifuged at 500 × g for 10 min at 4°C. The resulting postnuclear supernatant was further centrifuged at 100,000 × g in a TL100.2 rotor by using a tabletop Beckman ultracentrifuge for 30 min at 4°C. The supernatant (cytosol) was subsequently used for immunoprecipitation studies, and the immunoprecipitates were processed for Western blot analysis and PIP kinase assays, as described (27). Briefly, PC12 cell cytosol (1 mg) was rotated for 2 h at 4°C with 20-μl protein G-Sepharose beads (bed volume) precoated either with an anti-PIPK1γ serum or with a control serum (10 μl). Beads were then pelleted with a brief centrifugation at 1,000 × g in a microfuge, washed four times with the lysis buffer supplemented with 1% Triton X-100, and eluted with 100 μl of SDS/PAGE sample buffer for 2 min at 95°C. One-fifth of the immunoprecipitated material was loaded on an SDS/7.5% PAGE, along with the starting material and the supernatants (60 μg), and processed for Western blotting analysis. Western blotting was performed by using a rabbit antiserum directed to the COOH-terminal noncatalytic region of mouse PIPK1γ-87 (dilution ratio of 1:1,000) and detected with an ECL kit (Amersham Pharmacia, Piscataway, NJ) according to the manufacturer's recommendations. For the lipid kinase assay, immunoprecipitated material underwent an additional wash in kinase buffer (25 mM Hepes, pH 7.4/150 mM KCl/2 mM $MgCl_2$/1 mM EGTA) before the kinase reaction (for 15 min at 37°C) in the presence of 10 μCi (1 Ci = 37 GBq) of [γ^{32}P]ATP/50 μM cold ATP/20 μg of brain phosphoinositide mixture (Sigma) in a final volume of 50 μl.

Fluorescence Microscopy. Chromaffin cells were observed under a PerkinElmer spinning disk confocal microscope with a Yokogawa head between 12–24 h after infection with an adenovirus expressing PH-GFP. Images were acquired through the center of the cells by using a ×60 and 1.4 numerical aperture water immersion lens (excitation at 488 nm with appropriate filters). Line traces were randomly drawn across the cells and the ratio of PM to cytosol fluorescence intensity was measured.

Electrophysiology. Conventional whole-cell recordings were performed with two to four MΩ pipettes, and an EPC-10 patch-clamp amplifier was used together with PULSE software (HEKA Electronics, Lambrecht/Pfalz, Germany). The external bathing solution contained 140 mM NaCl, 2.8 mM KCl, 5 or 10 mM $CaCl_2$ (5 mM for RRP refilling assays and 10 mM for RRP measurements), 1 mM $MgCl_2$, 10 mM Hepes, and 5 mM glucose (pH 7.2, 310–320 mOsm), and the cells were perfused with the external bathing solution at a rate of 1–2 ml/min. The pipette solution contained 135 mM Cs-Glu, 2.8 mM KCl, 1 mM $MgCl_2$, 10 mM Hepes, 2 mM Mg ATP, and 0.3 Na_3GTP (pH 7.2, 290–300 mOsm), and ATP and GTP were added freshly. Basal $[Ca^{2+}]_i$ was buffered by a combination of 2 mM $CaCl_2$ and 5 mM EGTA to give a final free $[Ca^{2+}]_i$ of ≈200 nM. A liquid junction potential of 15.7 mV was corrected for all experiments. Capacitance measurements were performed by using the software lock-in module of PULSE. A 1-kHz, 40-mV peak-to-peak sinusoid stimulus was applied on a DC potential of −90 mV. The resulting current was processed by using the Lindau–Neher technique (28) to give estimates of the equivalent circuit parameters (C_m, G_m, and G_s). The reversal potential of the measured DC current was assumed to be 0 mV. ΔC_m values were analyzed with IGOR software (WaveMetrics, Lake Oswego, OR).The size of the RRP was estimated by using a dual-pulse protocol, in which the depolarizing potentials used for each pulse were selected to result in the same total Ca^{2+} influx. Typically, values of 0 mV for the first depolarization and +10 mV for the second depolarization were used. C_m was averaged over a 50-ms predepolarization segment to give a baseline value. Pilot experiments suggested that the transient gating capacitance artifact was negligible 40 ms after the end of a depolarization, thus, C_m was averaged over the 40- to 100-ms interval after depolarization, and the baseline C_m value was subtracted to obtain ΔC_m. Evoked Ca^{2+} currents were measured under conditions in which the majority of the K^+ currents were blocked by intracellular Cs^+. Tetrodotoxin was not used to block Na^+ conductance in these experiments because it has been shown to prolong nonsecretory capacitance transients in chromaffin cells. Instead, the first 10 ms of evoked inward current was ignored in estimations of Ca^{2+} influx. No correction for leak currents was made and cells with a leak of >150 pS were discarded.

EM. Fresh adrenal glands were isolated from newborn WT and KO mice and fixed with 2.5% paraformaldehyde and 3% glutaraldehyde in 0.1 M cacodylate buffer (pH 7.4) for 2 h at room temperature. Adrenals were then washed three times for 20 min with 0.1 M cacodylate buffer (pH 7.4), postfixed for 2 h at room temperature with 1% OsO_4 in 0.1 M cacodylate buffer (pH 7.4), dehydrated through a series of increasing ethanol concentrations, and embedded in Epon. Ultrathin sections (≈60 nm) were collected on formvar-coated stainless steel grids and stained with lead citrate and uranyl acetate, and the sections were observed with a TECNAI 12 (Philips/FEI, Hillsboro, OR) electron microscope. Chromaffin cells were identified by the presence of LDCVs, and the random images of chromaffin cells were acquired from three difference animals (and five different grids per animals) for both genotypes at ×4,200 magnification.

Automatic Detection and Analysis of LDCVs. A customized program (available on request) for MATLAB software (Mathworks, Natick, MA) was used to automatically detect, segment, and quantify LDCV parameters from EM images. All detection and analysis was performed in a double-blind manner. An open-by-reconstruction top-hat function with a circular structuring element of an eight-pixel radius (≈230 nm) was used to identify the electron-dense LDCVs (29). Analysis of the shape (symmetry) was based on normalized marginal central moments (skewness, kurtosis, and variability) of the gray level distributions in the principal axis of each candidate resulted in the final segmentation. Granule radius, area, and distance were automatically obtained; the distance was measured between the proximal side of the LDCV and the PM.

Amperometry. Carbon fibers with a diameter of 5 μm (ALA Scientific Instruments, Westbury, NY) were used for amperometry. Fibers were held at +700mV (30), and the tip of a freshly cut fiber was gently pressed against the cell. Currents were amplified and filtered at 3 kHz by an EPC-7 amplifier (HEKA Electronics) with a sampling rate of 4 kHz. Currents were digitally filtered at 500 Hz (Gaussian filter) and analyzed by a customized macro for IGOR PRO software. The following criteria were set in single-spike analysis: (*i*) only spikes larger than 10 pA were considered, (*ii*) the maximum number of spikes analyzed per cell was set to 150, (*iii*) foot duration was delimited by the baseline and spike onset (see Fig. 4*G Inset*), and (*iv*) spikes with a foot duration of <0.5 ms were excluded for the assays. When calculating spike frequency, spikes larger than 5 pA were included.

Generation of Adenoviruses. An adenovirus encoding the PH domain of PLCδ1 was a kind gift of O. Weisz (University of Pittsburgh, Pittsburgh) (31). An adenovirus encoding GFP was kind gift of Roland Baron (Yale University School of Medicine) (32). Adenovirus-encoding human PIPKIγ (87-kDa isoform) tagged with yellow fluorescent protein at the NH2 terminus was generated by a double-insert ligation. The cDNA of human PIPKIγ together with the cDNA-encoding yellow fluorescent protein were cloned into pShuttle-CMV (AdEasy, Stratagene), a vector for adenovirus. Specifically, PCR-amplified yellow fluorescent protein, carrying a *Bam*HI restriction site at the 5′ end, and an *Eco*RI restriction site at the 3′ end, was inserted together with full-length PIPKIγ cDNA digested by *Eco*RI/*Sal*I into the pShuttle-CMV vector, previously cut by *Bgl*II/*Sal*I. Adenovirus-encoding PIPKIγ was subsequently generated following the manufacturer's instructions (AdEasy, Stratagene).

Results

Expression of PIPKIγ in Adrenal Chromaffin Cells. Of the three catalytically active type I PIP kinases (α, β, and γ), the γ isoform (PIPKIγ) is the predominant isoform in neuronal tissue, where it accounts for a large fraction of $PI(4,5)P_2$ synthesis (24, 33). The availability of PIPKIγ KO mice (26), which die shortly after birth, offers the possibility to directly examine the importance of $PI(4,5)P_2$ synthesis mediated by this enzyme in LDCV secretion from isolated primary chromaffin cells, a neuroendocrine cell type. These cells, which are optimally suited for the biophysical analysis of secretion by capacitance and amperometric studies, allow for the dissection of the precise kinetic steps at which $PI(4,5)P_2$ synthesis is important.

As expected, given the neuroendocrine properties of chromaffin cells, PIPKIγ is expressed at significant levels in adrenal glands of newborn WT mice, as revealed by Western blotting (Fig. 1*A*). In contrast, no PIPKIγ immunoactivity was observed in adrenals from KO mice (Fig. 1*A*). Direct analysis of PIP kinase activity and $PI(4,5)P_2$ levels specifically in the chromaffin cells could not be performed because of the low number of these cells. However, an indirect estimate of the levels of $PI(4,5)P_2$ in the PM of chromaffin cells freshly isolated from neonatal glands could be obtained by adenovirus-mediated expression of the PH domain of PLCδ1 fused to GFP. This fusion protein binds $PI(4,5)P_2$ at the PM and functions as a quantitative detector of this phosphoinositide in fluorescent images (34). The intensity of the GFP fluorescence associated with the PM relative to the cytosolic fluorescence was much lower in KO chromaffin cells than in WT cells (Fig. 1 *B* and *C*), demonstrating the occurrence of lower $PI(4,5)P_2$ levels on the PM of KO cells.

Expression of PIPKIγ in chromaffin cells was further confirmed by the analysis of undifferentiated PC12 cells, a chromaffin cell line that is a well established model for studies of exocytosis (35, 36). A prominent PIPKIγ-immunoreactive band was detected by Western blotting in extracts of these cells (Fig. 1*D*) and an anti-PIPKIγ antiserum-precipitated PIP kinase activity from such extracts (Fig. 1*E*). Both mouse adrenal gland and PC12 cells, in contrast to brain, contained mainly the short PIPKIγ isoform (87 kDa), which lacks the talin-binding site (Fig. 1*D* and data not shown) (27).

Smaller RRP of LDCVs in PIPKIγ-Deficient Chromaffin Cells. Secretion studies were carried out on primary chromaffin cells from newborn WT and KO mice. Cells were stimulated with a dual-pulse depolarization protocol (Fig. 2*A*), and Ca^{2+} current and membrane capacitance were simultaneously monitored before and after stimulation. Depolarization induced a robust increase in membrane capacitance in WT cells (black lines, Fig. 2*A Upper*), reflecting the exocytosis of secretory granules (37, 38). The secretory response was markedly reduced in KO cells

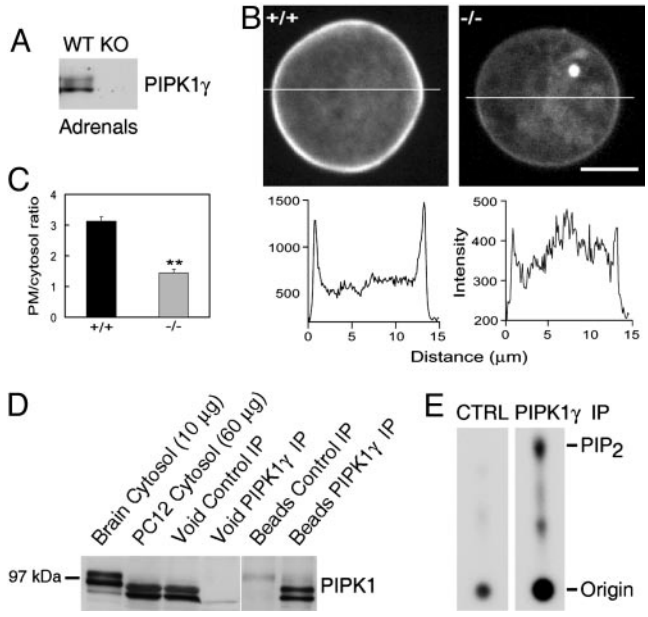

Fig. 1. PIPKIγ is expressed in chromaffin cells and plays a key role in the maintenance of normal $PI(4,5)P_2$ levels at the PM. (*A*) Western blot demonstrating the expression of PIPKIγ in adrenal extracts (10 μg) prepared from newborn animals. PIPKIγ immunoreactivity is absent in KO adrenals. Equal amounts (10 μg) of WT and KO material were loaded on the SDS/PAGE. (*B*) WT and KO chromaffin cells were infected with PH-GFP and imaged (*Upper*) on a spinning disk confocal microscope through the center of the cells. Line profiles (*Lower*) show the relative intensity of fluorescence across the cells. (*C*) Analysis of several cells revealed a significant decrease (**, $P < 0.01$) in the PM/cytosol fluorescence ratio in KO ($n = 13$) compared with WT ($n = 15$) cells, indicating a lower PM associated $PI(4,5)P_2$ level in the KO cells. (*D*) Western blot analysis of cytosolic extracts of rat brain (lane 1) and PC12 cells (lane 2), and of void and pellet fractions of anti-PIPKIγ immunoprecipitates from PC12 cells (lanes 3–6). Chromaffin cells express primarily the short isoform of PIPKIγ (87 kDa), thus explaining the faster migration of PIPKIγ-immunoreactive bands in PC12 cells. (*E*) Presence of PIP kinase activity in anti-PIPKIγ and control (CTRL) immunoprecipitates generated from PC12 cells. Immunoprecipitates were incubated with [γ^{32}P]ATP and a phosphoinositide mixture, and the products of the reaction were separated by TLC followed by autoradiography. The difference in spot size at the origin reflects uneven washout of residual [γ-^{32}P]ATP and is not relevant to the difference observed on the PIP2 spot.

(gray lines, Fig. 2*A Upper*), whereas the calcium currents were identical to WT cells (Fig. 2 *A Lower* and *B*).

Data from the dual-pulse protocol was used to calculate the size of the RRP of LDCVs (37, 38). The RRP, a kinetically defined parameter, is generally considered as the penultimate step in vesicle fusion, and is believed to reflect vesicles already docked to the PM in a fusion-competent state. When the two depolarizations are given in rapid succession (e.g., a 100-ms delay), the RRP, B_{max}, can be derived from the equation: $B_{max} = S/(1 - R^2)$, assuming that the release probability is the same for the first and second stimulus (37). *S* represents the sum of the capacitance responses to the first (ΔC_1) and the second (ΔC_2) depolarization, and *R* is defined as the ratio of $\Delta C_2/\Delta C_1$, which reflects the fraction of LDCVs in the RRP mobilized by stimulation. Analysis showed that *R* values were similar for WT and KO chromaffin cells (Fig. 2*C*), implying that PIPKIγ depletion does not change the release rate. However, the size of the RRP in the KO cells was only 40% of that in WT cells (Fig. 2*D*).

To investigate the refilling kinetics of the RRP, we applied a second dual-pulse stimulation at various time intervals after the first protocol (37, 39). The refilling kinetics can be estimated by a linear regression fit of the log of the interpulse interval versus the B_{max} of the second stimulation (Fig. 2*E*). The slope, *m*, for

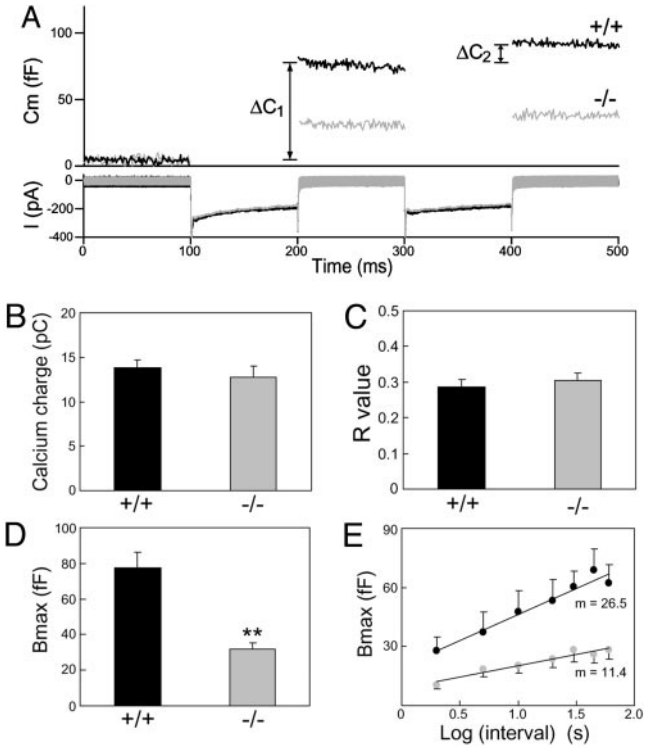

Fig. 2. The RRP was reduced and exhibited slower refilling kinetics in KO chromaffin cells as measured by whole-cell capacitance studies. (*A*) Changes in capacitance (Cm, upper trace) and Ca^{2+} current (I, lower trace) were simultaneously monitored in response to a dual-depolarization protocol. (*B* and *C*) The Ca^{2+} influx in *B* (WT, 13.8 ± 0.9 pC; KO, 12.8 ± 1.2 pC) and the ratio $R = \Delta C_1/\Delta C_2$ in *C* (WT, 0.29 ± 0.02; KO, 0.31 ± 0.02) were similar in WT (black bar) and KO (gray bar) cells. (*D*) The size of the RRP (B_{max}) in KO cells (gray bar) was only 40% of that in WT cells (black bar) (WT, 77.5 ± 9.1 fF; KO, 31.8 ± 3.3 fF). Data were averaged from 30 cells from seven WT mice and 29 cells from six KO mice. (*E*) To monitor the RRP refilling kinetics, RRP (B_{max}) was plotted against the $\log_{10}$ of the interpulse intervals (black circles for WT and gray circles for KO). Ten to 16 cells were examined for all intervals tested. Data were presented as mean ± SEM. **, $P < 0.01$.

KO cells ($m = 11.4$) was much smaller than that for WT cells (m = 26.5), demonstrating an ≈55% decrease in the refilling kinetics of the RRP in KO cells.

Absence of an LDCV Docking Defect. These data show a clear secretion defect in KO chromaffin cells when PIPKIγ is absent. To determine whether the defect resulted from a change in either the total number of LDCVs or their intracellular distribution, or both, an EM of the adrenals was performed (an example from WT is shown in Fig. 3*A*, and its analysis is shown in Fig. 3*B*). No gross morphological difference was observed between WT and PIPK1γ KO chromaffin cells (data not shown). A morphometric analysis, carried out for each group by blind automated granule detection and quantification on ≈40 cells and ≈3,000 granules (WT and KO), revealed that the size distribution of LDCVs was identical for both genotypes (Fig. 3*C*). Furthermore, similar numbers of granules per cell cross section (Fig. 3*D*) and unit area of cytosol were observed (Fig. 3*E*); these values were similar to those reported elsewhere (40). Although the decrease in the RRP could predict fewer docked LDCVs, a small but significant increase in the number of LDCVs that are within 100 nm from the PM was observed in KO cells (Fig. 3*F*). These results indicate that the decreased secretion observed in the capacitance studies was not due to a change in the size or number of granules. Rather, they suggest that an event downstream of morphological docking is impaired in the KO chromaffin cells.

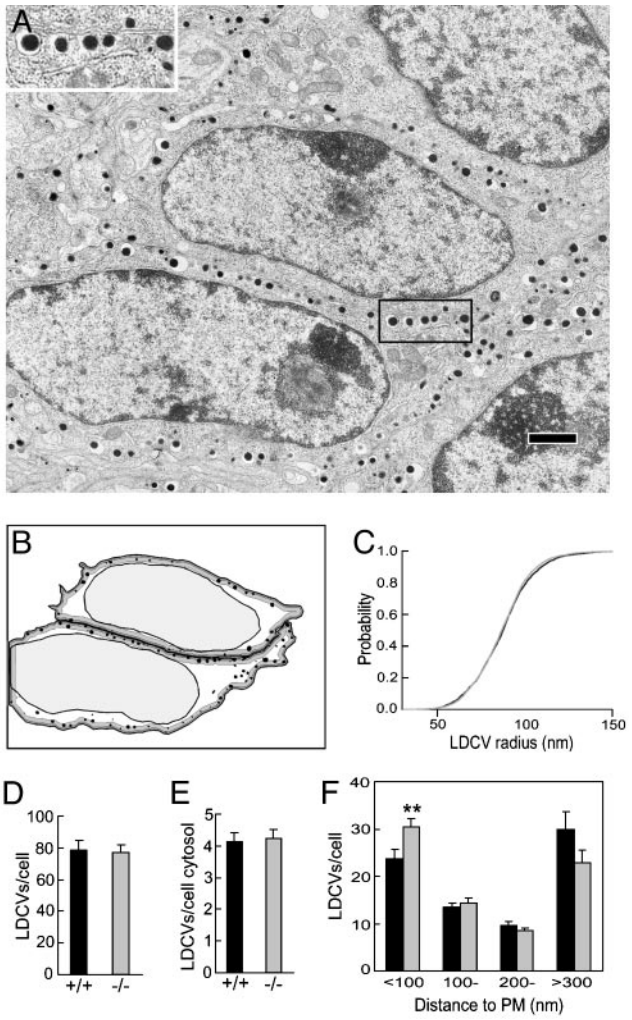

Fig. 3. EM morphometric analysis of LDCVs in WT and KO chromaffin cells. (*A*) Micrograph of an adrenal section from a KO mouse. (*Inset*) Expanded view of LDCVs in close proximity, docked, to the PM. (Bar, 1 μm.) (*B*) Cartoon showing automatic LDCV detection and quantification of cells in *A* (see *Materials and Methods*). The dark and light gray zone represents a distance of 100 and 300 nm from the PM, respectively. (*C–E*) The LDCV size (*C*; normalized cumulative distribution), total number of LDCVs per cell cross section (*D*), and per area of cytosol (*E*) were identical in WT (black bar) and KO (gray bar) cells. (*F*) A small but significant (**, $P < 0.01$) increase in fraction of granules was closer to the PM (<100 nm) in KO cell (gray bar) than in WT cells (black bar). Data were presented as mean ± SEM.

Decreased Exocytic Burst of Individual LDCVs in Response to Ca^{2+}. To determine whether PIPKIγ is involved in the final step of exocytosis (membrane fusion), the aforementioned capacitance studies were complemented by analysis of catecholamine release from single LDCVs by using carbon fiber amperometry (30). In these experiments, secretion from patched cells was recorded by using a carbon fiber placed in direct contact with the cells. Patch rupture and consequent influx of cytosolic buffer containing 10 μM Ca^{2+} resulted in robust secretion from both WT and KO cells (Fig. 4*A*). However, the frequency of amperometric spikes during the first minute after stimulation in KO cells was only 70% of WT cells (Fig. 4*B*), confirming an impaired exocytosis in KO cells.

The importance of $PI(4,5)P_2$ synthesis in the exocytic burst was

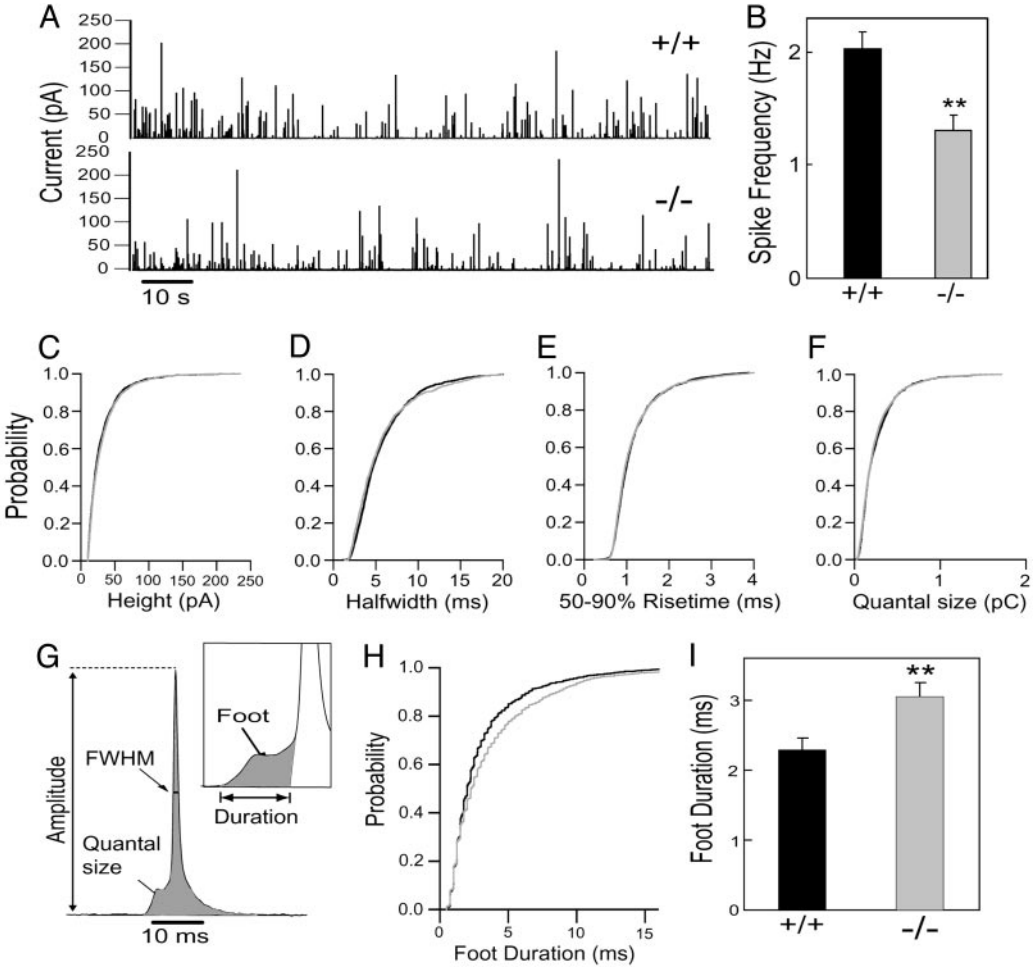

Fig. 4. Longer fusion pore duration in KO chromaffin cells. (*A*) Amperometric detection of catecholamine secretion from WT (*Upper*) and KO (*Lower*) chromaffin cells stimulated with 10 μM Ca^{2+} through the patch pipette. Each amperometric spike represents the fusion of an individual granule. (*B*) Spike frequency for WT (black bar) and KO cells (gray bar). (*C–F*) Normalized cumulative distributions for: the peak amplitude (*C*), half-width (FWHM, full width of half maximum) (*D*), 50–90% rise time (*E*), and quantal size (*F*). (*G*) Diagram of the parameters analyzed in amperometric spikes. (*H* and *I*) Analysis of foot duration. Normalized cumulative distributions of all events in all cells (*H*) and average of median values obtained from individual WT (black bar) and KO (gray bar) cells (*I*). Data in *B* and *H* are expressed as mean ± SEM; 23 WT and 30 KO cells were analyzed (also see Table 1). **, $P < 0.01$.

confirmed by amperometric measurements of secretion in WT chromaffin cells after adenovirus-mediated overexpression of yellow fluorescent protein-tagged PIPKIγ. As previously shown, overexpression of this PIPKIγ leads to a robust increase in $PI(4,5)P_2$ levels (41). The frequency of amperometric spikes during the first minute after stimulation was 20% higher in cells overexpressing PIPKIγ than in cells overexpressing only GFP (2.45 ± 0.12 for PIPKIγ and 2.01 ± 0.14 for GFP).

Delay in Fusion Pore Expansion. Amperometry can also provide detailed millisecond information about the kinetics of catecholamine release from individual granules, and allows resolution of the initial release through a transient fusion pore, the foot signal, from the subsequent spike of catecholamine release (Fig. 4*G*). No noticeable differences were observed between spikes of WT and KO cells in a variety of parameters, including peak amplitude (Fig. 4*C*), half-width (Fig. 4*D*), 50–90% rise time (Fig. 4*E*), and the quantal size (Fig. 4*F*), which is the integration of the total amperometrical current. The fraction of spikes with feet was also unchanged in KO cells (86.5 ± 1.5 for WT and 89.1 ± 1.3 for KO). However, a significant difference was observed in the duration of the foot, with a longer foot being observed in KO

Table 1. Characteristics of single fusion events as detected by amperometry

			Cell medians				
	No. of cells	No. of events	Amplitude, pA	Quantal size, pC	Half-width, ms	Rise time, ms	Foot duration, ms
WT	23	1,575	24.9 ± 2.2	0.24 ± 0.02	5.19 ± 0.32	1.05 ± 0.05	2.28 ± 0.18
KO	30	1,476	24.0 ± 1.3	0.25 ± 0.02	5.15 ± 0.31	1.11 ± 0.05	3.05 ± 0.21*
PIPK Iγ	21	1,613	25.8 ± 1.3	0.26 ± 0.02	5.36 ± 0.39	1.19 ± 0.07	2.38 ± 0.11
GFP	24	1,429	26.5 ± 1.6	0.27 ± 0.02	5.46 ± 0.32	1.12 ± 0.04	2.46 ± 0.11

Data are presented as mean ± SEM of the cell median for each parameter. Thus, the numbers used for the calculation of the SEM and the statistical tests are the median for each cell. Differences between WT and KO in all parameters were nonsignificant, except for the foot duration. *, $P < 0.01$.

cells (Fig. 4 *H* and *I* and Table 1), suggesting that $PI(4,5)P_2$ regulates fusion pore dynamics. Interestingly, synaptotagmin, a protein that has been proposed to regulate fusion pore dynamics (35, 36), binds phosphoinositides and in particular $PI(4,5)P_2$ (8–10). This lipid may also control fusion pore dynamics indirectly, by means of effects on the actin cytoskeleton (1, 4, 42), and therefore, on the tension of the PM that surrounds exocytic sites. No detectable differences were observed between cells overexpressing PIPKIγ or expressing GFP in the kinetics of LDCVs fusion, including foot duration, indicating that $PI(4,5)P_2$ at the physiological concentration is not rate-limiting for this process (Table 1).

Discussion

Collectively, these findings prove the physiological importance of $PI(4,5)P_2$ synthesis in LDCV exocytosis. In agreement with the neuroendocrine properties of chromaffin cells, our study identifies PIPKIγ, the major neuronal type I PIP kinase isoform [i.e., the major neuronal PI(4)P 5-kinase], as a key PIP enzyme regulating this process in chromaffin cells. Clearly, $PI(4,5)P_2$ is only expected to be decreased, but not absent, in PIPKIγ-deficient chromaffin cells, as also shown by studies on neurons from PIPKIγ KO mice (26). Other PIP kinases are expected to be expressed in these cells, including other type I PIP kinases (24, 25). Our findings demonstrate that the $PI(4,5)P_2$ pool controlled by PIPKIγ plays an important role in regulating the size of the secretory response and the kinetics of fusion pore expansion.

PIPKIγ KO cells exhibit a decrease in the RRP of LDCVs and in the refilling rate of this pool relative to WT cells. This result is in agreement with a decrease of the RRP of synaptic vesicles at neuronal synapses of PIPKIγ KO mice, and thus, suggests yet another mechanistic similarity between synaptic vesicle and LDCV exocytosis. The reduction in the RRP of LDCVs does not correlate with a parallel decrease in the number of docked LDCVs, which are in fact more numerous than in WT. Furthermore, the decreased exocytic response cannot be attributed to an impaired Ca^{2+} signaling from PIPKIγ-deficient cells, because Ca^{2+} currents were unchanged in the capacitance studies, and the Ca^{2+} concentration was clamped in the amperometric studies.

These results strongly point to a defect in vesicle priming in PIPKIγ-deficient cells. Thus, they provide direct genetic evidence for the importance of PI(4)P phosphorylation in the ATP-dependent priming of LDCVs, as predicted more than a decade ago by studies on broken cell preparations (5, 6). Although these earlier reports and subsequent studies (5, 6) have indicated a direct role of $PI(4,5)P_2$ in LDCV priming, more recent studies have also implicated its metabolite diacylglycerol in this reaction by means of its interaction with Munc13/Unc13 (19–22). An attractive possibility is that the secretory defects observed here may be related to a decrease of both $PI(4,5)P_2$ and diacylglycerol as a consequence of impaired $PI(4,5)P_2$ synthesis.

We thank Lijuan Liu for technical assistance, Drs. Jennifer Morgan and Jeff Sfakianos for critical readings of the manuscript, Drs. Eugene Mosharov and Roland Staal (D. Sulzer Laboratory, Department of Neurology, Columbia University, New York) for the Igor macro used for amperometric data analysis, Dr. Ora Weisz for the generous gift of adenovirus-expressing GFP fused to the PH domain of PLCδ1, and Dr. Roland Baron for the generous gift of adenovirus-expressing GFP. This work was supported in part by Human Frontier Science Program Grant RGY0040/2003 (to L-W.G., M.-E.D., and D.T.), Yale Diabetes Endocrinology Research Center 2004 Pilot Grant (to G.D.P.), and National Institutes of Health Grants NS36251 and DK45735 (to P.D.C.).

1. Martin, T. F. (2001) *Curr. Opin. Cell Biol.* **13,** 493–499.
2. Simonsen, A., Wurmser, A. E., Emr, S. D. & Stenmark, H. (2001) *Curr. Opin. Cell Biol.* **13,** 485–492.
3. De Matteis, M. A. & Godi, A. (2004) *Nat. Cell Biol.* **6,** 487–492.
4. Wenk, M. R. & De Camilli, P. (2004) *Proc. Natl. Acad. Sci. USA* **101,** 8262–8269.
5. Eberhard, D. A., Cooper, C. L., Low, M. G. & Holz, R. W. (1990) *Biochem. J.* **268,** 15–25.
6. Hay, J. C., Fisette, P. L., Jenkins, G. H., Fukami, K., Takenawa, T., Anderson, R. A. & Martin, T. R. (1995) *Nature* **374,** 173–177.
7. Jahn, R. & Sudhof, T. C. (1999) *Annu. Rev. Biochem.* **68,** 863–911.
8. Schiavo, G., Gu, Q. M., Prestwich, G. D., Sollner, T. H. & Rothman, J. E. (1996) *Proc. Natl. Acad. Sci. USA* **93,** 13327–13332.
9. Shin, O. H., Rizo, J. & Sudhof, T. C. (2002) *Nat. Neurosci.* **5,** 649–656.
10. Bai, J., Tucker, W. C. & Chapman, E. R. (2004) *Nat. Struct. Mol. Biol.* **11,** 36–44.
11. Renden, R., Berwin, B., Davis, W., Ann, K., Chin, C. T., Kreber, R., Ganetzky, B., Martin, T. F. & Broadie, K. (2001) *Neuron* **31,** 421–437.
12. Loyet, K. M., Kowalchyk, J. A., Chaudhary, A., Chen, J., Prestwich, G. D. & Martin, T. F. (1998) *J. Biol. Chem.* **273,** 8337–8343.
13. Holz, R. W., Hlubek, M. D., Sorensen, S. D., Fisher, S. K., Balla, T., Ozaki, S., Prestwich, G. D., Stuenkel, E. L. & Bittner, M. A. (2000) *J. Biol. Chem.* **275,** 17878–17885.
14. Lawrence, J. T. & Birnbaum, M. J. (2003) *Proc. Natl. Acad. Sci. USA* **100,** 13320–13325.
15. Honda, A., Nogami, M., Yokozeki, T., Yamazaki, M., Nakamura, H., Watanabe, H., Kawamoto, K., Nakayama, K., Morris, A. J., Frohman, M. A. & Kanaho, Y. (1999) *Cell* **99,** 521–532.
16. Krauss M., Kinuta, M., Wenk, M. R., De Camilli, P., Takei, K. & Haucke, V. (2003) *J. Cell Biol.* **162,** 113–124.
17. Aikawa, Y. & Martin, T. F. (2003) *J. Cell Biol.* **162,** 647–659.
18. Vitale, N., Chasserot-Golaz, S., Bailly, Y., Morinaga, N., Frohman, M. A. & Bader, M. F. (2002) *J. Cell Biol.* **159,** 79–89.
19. Ashery, U., Varoqueaux, F., Voets, T., Betz, A., Thakur, P., Koch, H., Neher, E., Brose, N. & Rettig, J. (2000) *EMBO J.* **19,** 3586–3596.
20. Richmond, J. E., Weimer, R. M. & Jorgensen, E. M. (2001) *Nature* **412,** 338–341.
21. Rhee, J. S., Betz, A., Pyott, S., Reim, K., Varoqueaux, F., Augustin, I., Hesse, D., Sudhof, T. C., Takahashi, M., Rosenmund, C. & Brose, N. (2002) *Cell* **108,** 121–133.
22. Varoqueaux, F., Sigler, A., Rhee, J. S., Brose N., Enk, C., Reim, K. & Rosenmund, C. (2002) *Proc. Natl. Acad. Sci. USA* **99,** 9037–9042.
23. Anderson, R. A., Boronenkov, I. V., Doughman, S. D., Kunz, J. & Loijens, J. C. (1999) *J. Biol. Chem.* **274,** 9907–9910.
24. Doughman, R. L., Firestone, A. J. & Anderson, R. A. (2003) *J. Membr. Biol.* **194,** 77–89.
25. Wang, Y. J., Li, W. H., Wang, J., Xu, K., Dong, P., Luo, X. & Yin H. L. (2004) *J. Cell Biol.* **167,** 1005–1010.
26. Di Paolo, G., Moskowitz, H. S., Gipson, K., Wenk, M. R., Voronov, S., Obayashi, M., Flavell, R., Fitzsimonds, R. M., Ryan, T. A. & De Camilli, P. (2004) *Nature* **431,** 415–422.
27. Di Paolo, G., Pellegrini, L., Letinic, K., Cestra, G., Zoncu, R., Voronov, S., Chang, S., Guo, J., Wenk, M. R. & De Camilli, P. (2002) *Nature* **420,** 85–89.
28. Lindau, M. & Neher, E. (1988) *Pflügers Arch.* **411,** 137–146.
29. Soille, P. (1999) *Morphological Image Analysis: Principles and Applications.* (Springer, New York).
30. Chow, R. H., von Ruden, L. & Neher, E. (1992) *Nature* **356,** 60–63.
31. Lee, E., Marcucci, M., Daniell, L., Pypaert, M., Weisz, O. A., Ochoa, G. C., Farsad, K., Wenk, M. R. & De Camilli, P. (2002) *Science* **297,** 1193–1196.
32. Miyazaki, T., Neff, L., Tanaka, S., Horne, W. C. & Baron, R. (2003) *J. Cell Biol.* **160,** 709–718.
33. Wenk, M. R., Pellegrini, L., Klenchin, V. A., Di Paolo, G., Chang, S., Daniell, L., Arioka, M., Martin, T. F. & De Camilli, P. (2001) *Neuron* **32,** 79–88.
34. Balla, T. & Varnai, P. (2002) *Sci. STKE.* **125**, PL3.
35. Wang, C. T., Grishanin, R., Earles, C. A., Chang, P. Y., Martin, T. F., Chapman, E. R. & Jackson, M. B. (2001) *Science* **294,** 1111–1115.
36. Wang, C. T., Lu, J. C., Bai, J., Chang, P. Y., Martin, T. F., Chapman, E. R. & Jackson, M. B. (2003) *Nature* **424,** 943–947.
37. Gillis, K. D., Mossner, R. & Neher, E. (1996) *Neuron* **16,** 1209–1220.
38. Smith, C, Moser, T., Xu, T. & Neher, E. (1998) *Neuron* **20,** 1243–1253.
39. Xu, T., Ashery, U., Burgoyne, R. D. & E. Neher, E. (1999) *EMBO J.* **18**, 3293–3304.
40. Sorensen, J. B., Nagy, G., Varoqueaux, F., Nehring, R. B., Brose, N., Wilson, M. C. & Neher, E. (2003) *Cell* **114,** 75–86.
41. Wenk, M. R., Lucast, L., Di Paolo, G., Romanelli, A. J., Suchy, S. F., Nussbaum, R. L., Cline, G. W., Shulman, G. I., McMurray, W. & De Camilli, P. (2003) *Nat. Biotech.* **21,** 813–817.
42. Yin, H. L. & Janmey, P. A. (2003) *Annu. Rev. Physiol.* **65,** 761–789.